ORIGINAL ARTICLE

The dependency of the microhardnes on microstructure and solidification parameters of directionally solidified Al–4.5wt.%Cu in clay mold

D. Masnur[1,2], V. Malau[1], Suyitno[1,3]*

[1] Mechanical and Industrial Engineering Department, Universitas Gadjah Mada, Jl. Grafika No. 2, Yogyakarta 55281, Indonesia
[2] Mechanical Engineering Department, University of Riau, Kampus Bina Widya km 12.5 Simpang Baru, Pekanbaru 28293, Indonesia
[3] Center Innovation for Medical Equipments Devices/CIMEDs, Universitas Gadjah Mada, Jl. Grafika No. 2, Yogyakarta 55281, Indonesia

ABSTRACT – Improvement of material properties is achieved by controlling parameters involved in the solidification process; therefore, understanding them and their implication are essential. This work investigated the dependency of solidification parameters (cooling rate (T_R), growth rate (V_L), local solidification time (t_{SL}), temperature gradient (G)), microstructure parameters (primary (λ_1) and secondary (λ_2) dendrite arm spacing), and micro-hardness values (HV) of Al-4.5wt.%Cu in the clay mold. The samples were directionally solidified in Bridgman vertical apparatus and the temperature is recorded during the cooling. The solidification parameters were obtained from the cooling curve. The microstructures and micro-hardness were characterized using an optical microscope and micro-hardness tester. The microstructure parameters were measured and plotted as functions of solidification parameters using linear regression. The relation between HV and microstructure parameters are analyzed. The results show the λ_1 and λ_2 change inversely with solidification parameters except for t_{SL}. Comparison to other works shows the exponent values of solidification parameters of the clay mold are lower than that of the carbon and stainless-steel mold. The exponent value of λ_2 in the clay mold is -0.183, close to the value in the graphite mold. The clay has the potential as mold material since it characteristic close to the graphite.

INTRODUCTION

The current technology needs advanced materials that can be applied for many purposes; for example, high strength to weight ratio materials is one of the requirements in material selection in the aircraft industry and marine applications [1]. The pure metal is not sufficient to meet the criteria; therefore, alloying becomes an option to improve material properties. The additions of copper in aluminum improves tensile strength and hardness in the cast and heat-treated products at room and elevated temperature [2,3]. Alloys containing 4 to 5.5wt.%Cu respond most strongly to thermal treatment and display relatively improved casting properties [4]. These improvements had brought a widespread usage of Al-Cu alloys in industry.

Improvements in material properties are also conducted by controlling the solidification parameters during the solidification. The preliminary stage is characterizing the solidification with the solidification parameters, e.g., cooling rate (T_R), local solidification time (t_{SL}), growth rate (V_L), and temperature gradient (G). Numbers of researchers investigated and analyzed the dependency of those parameters on the microstructure parameters (primary dendrite arm spacings (λ_1) and secondary arm spacings (λ_2)) and micro-hardness of Al-Cu alloys. A few numbers of compositions were investigated, such as 3, 5, 6, 8, 10, 15, and 24 wt.% [5–9] and commonly used mold material was stainless steel [5,8,9]. The samples were cooled at the bottom without any heat supply from the furnace. However, in practice, the mold materials are varied, and it affects the solidification parameters as well as microstructure parameters [10,11]. Explorations regarding composition, mold materials, and treatment during the cooling are still needed to provide extensive information in understanding the relation between solidification parameters, microstructure parameters, and micro-hardness.

Hardness is commonly related to the microstructure formation; therefore, the investigations of their relationship have been carried out intensively. Hall-Petch (HP) had formulated the correlation in the form of experimental and the simplified one as follows accordingly [6]:

$$HV = H_0 + k\lambda_{(1,2)}^{-0.5} \tag{1}$$

$$HV = k\lambda_{(1,2)}^{-n} \tag{2}$$

where, H_0 and k are experimental constant, and n is the exponent value for λ_1 and λ_2. The proposed HP equations of Al-Cu alloys from previous works are generally conducted under a vertical upward method and graphite mold. The studied compositions of Cu were 3, 6, 15, and 24 wt.%. The exponent values of λ_2 of the HP expression are reported in the range of -0.15 to -0.21. Providing HP expression for different compositions and mold material would help in a comprehensive understanding of microstructure and micro-hardness relationship.

This work investigates experimentally the dependency of solidification parameters, microstructure parameters (λ_1 and λ_2) and micro-hardness of directionally solidified Al−4.5wt.% Cu in the clay mold. Also, micro-hardness dependency on the microstructural relation is proposed.

METHODS AND MATERIALS

AA1050 and Al–40 wt.% Cu were mixed by a weighed amount in an electrical furnace at 700°C to prepare Al–4.58wt.%Cu samples. The melt was cast into a medium carbon steel mold with six cylindered shapes die cavities. The size of the holes was 6 mm diameter and 60 mm in length. The cylinder was inserted into a hollow cylinder clay mold. The size of the clay mold was 10 mm outside diameter, 6 mm inside diameter and 60 mm length. It was made with six holes with 0.75 mm diameter. The first hole located at 5 mm from the bottom and the next ones had a 10 mm distance and 60° angle between them, as illustrated in (Figure 1a). The clay thermal conductivity was 12.75 W/m.K (laboratory tested).

An acquisition apparatus with a computer recorded the temperature data through the six embedded thermocouples in the six holes. The sample was positioned in a heating chamber, as illustrated in Figure 1(b). Electric heater raised the sample temperature to 700°C at 1.9°C/s constant rate, and the temperature was held for 10 minutes. Next, the sample was being moved downward 0.04 mm/s while it was cooled at the bottom by the cooling system. The furnace was still active during the cooling to maintain the solidification only in the vertical direction. The temperature recording was stopped when the sample was out of the heating chamber. An acquisition apparatus with PLX-DAQ and Arduino Uno system recorded the temperatures during the cooling.
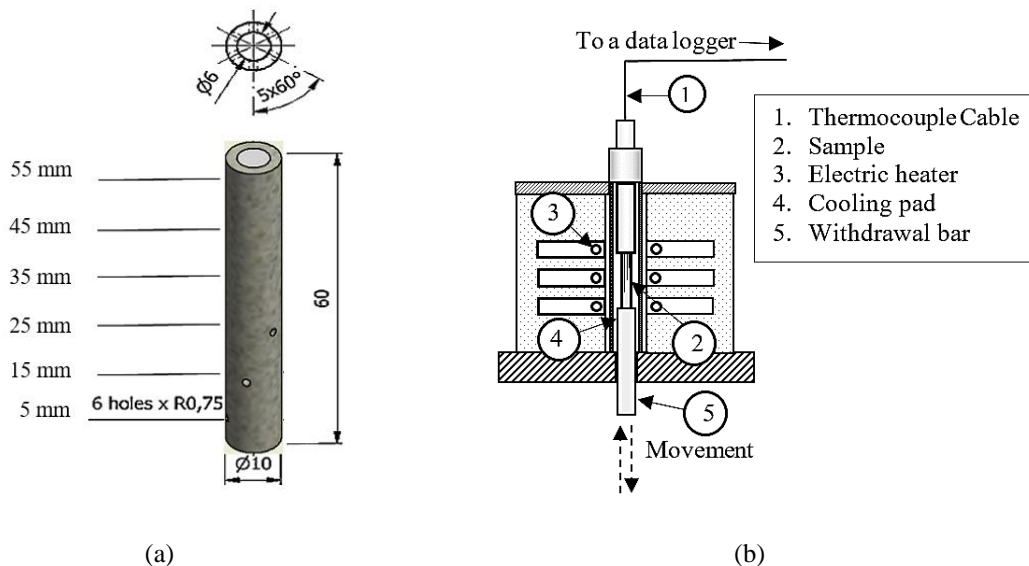
Figure 1. (a) Clay molds and holes position details and (b) scheme of equipment

The cooling curve is created using temperatures to time data. The liquidus and solidus temperature at selected composition (4.5%Cu) was 648.7°C and 561.3°C [12,13]. The cooling rate, local solidification time, temperature gradient, and the growth rate are calculated on each curve between these temperatures. The cooling rate is the slope of the cooling curve between the liquidus temperature and the solidus temperature) [14,15]. The discrepancy of liquidus and solidus time is defined as the local solidification time [16]. The temperature gradient was the measured value of temperatures difference of two thermocouples dividing by their distance [17]. The growth rate was the division of the distance of two thermocouples by the time taken by the solid-liquid interface to reach the second thermocouple. The local solidification times was the transforming time from liquid to solid in each thermocouple [7].

The samples were sectioned parallel to its length, and then the metallography sample's preparation procedures were applied. 1% HF aqueous solution was applied to the polished surface to reveal the microstructure [18]. Observation for microstructure was conducted by using an optical microscope. The primary dendrite arm spacing (λ_1) was gained by measuring the distance between the center of the nearest two dendrites trunks on the longitudinal section [7,17]. The secondary dendrite arm spacing (λ_2) were the average distance of the adjacent side branches of the longitudinal section of a primary dendrite. Both λ_1 and λ_2 reported here are taken from the average of five measurements. The obtained λ_1 and λ_2 values are plotted as functions of solidification parameters. Linear regression analysis was used to describe the mathematical relationship between those parameters, e.g., $\lambda_1 = k.G^a$ [7]. Micro-hardness values were measured with Boehler micro-hardness using 50g load and 10s dwelling time [7,19]. The micro-hardness values were taken in a 5 mm interval started from 5 mm and ended at 50 mm. Three indentations were made in each selected distance. The obtained

micro-hardness data was plotted to establish the Hall–Petch (HP) type relationship between distance from heat extraction point, λ_1, and λ_2 to micro-hardness (HV), respectively [6].

RESULTS AND DISCUSSION

Microstructure Parameters

Figure 2 depicts the mean values of λ_1 and λ_2 as the function of the cooling rate, the growth rate, the local solidification time, and the temperature gradient, respectively. The values of λ_1 and λ_2 change inversely to T_R, V_L, and G except for t_{SL}. The λ_1 and λ_2 values are decreasing from 66.08 to 23.42 µm and 26.96 to 11.08 µm accordingly with the increasing of T_R from 0.06 to 2.41°C/s.
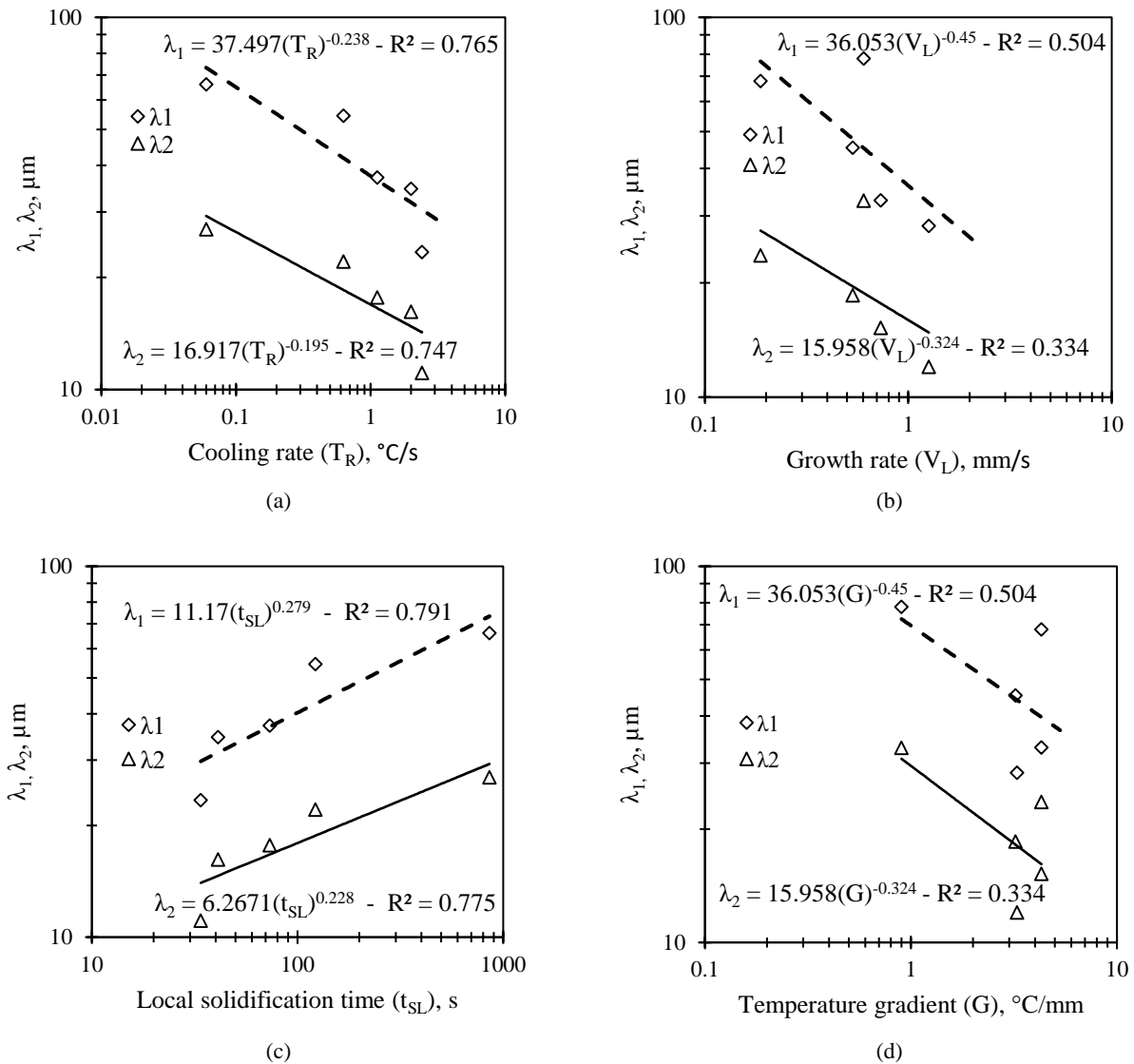
Figure 2. Plotting data of the average of λ_1 and λ_2 as the function of: (a) cooling rate (T_R), (b) growth rate (V_L), (c) local solidification time (t_{SL}) and (d) temperature gradient (G)

The exponent values of T_R for λ_1 and λ_2 are -0.238 and -0.195. The λ_1 and λ_2 values also decreasing with the increasing growth rate from 0.6 to 1.26 mm/s. In contrast, the λ_1 and λ_2 values increase with the local solidification time from 33.85 to 857.89s. The exponent values of T_R, V_L, t_{SL}, and G for λ_1 and λ_2 are -0.238 and -0.195, -0.045 and -0.324, 0.279, and 0.228, and -.045 and -0.324 accordingly.

The high value of T_R, V_L, and G are obtained at the beginning of the cooling process. These values associated with a massive heat transfer, which transforms the liquid into the solid in a short time. The heat flow is mainly in the vertical direction, and the grain grows to the opposite. Fine grains with short secondary branches are formed (Figure 3a). These grains have a minimum spacing (λ_1 and λ_2). As the T_R, V_L, and G gradually decrease, the grains are thickening, and the secondary branches grow, contributing more space between the grains (Figure 3b). Some of the secondary branches block the primary dendrite path and stop the growth of the primary dendrite. Finally, at the minimum value of T_R, V_L, and G,

the selected primary dendrites fill the unoccupied space; they grow in size with long secondary branches, but their number is less (the λ_1 and λ_2 are at maximum) (Figure 3c). The increasing of λ_1 and λ_2 with the decreasing of G and V_L also found by [7]. This phenomena also reported by [9,20] in the form of the thermal conductivity coefficient reduction.

There is still no investigation on Al−4.5 wt.% Cu; hence, the comparison to previous works is made with other closest compositions in the same alloy system (Table 1 and Table 2). The value of cooling rate exponent of λ_1, -0.238 is 0.312 lower than the one observed by [5,8] for Al−3 wt.% Cu and Al−6 wt.% Cu with stainless steel mold respectively. The cooling rate exponent value of λ_2, -0.195 is lower than -1/3, the one reported by [6,8], for Al−3wt.% Cu and Al−6 wt.% Cu with the carbon steel and the stainless steel mold. The λ_2 exponent values of growth rate, -0.324 is lower than the exponent values of Al−3 wt.% Cu in the carbon steel mold, -2/3 [6]. The λ_2 exponent values related to the local solidification time, 0.228 is higher than the exponent of the previous works, 1/3 [5,6]. Moreover, the λ_2 exponent values of the temperature gradient, -0.324 is below -0.39 and -0.62, the temperature gradient exponent value of Al−3wt.% Cu and Al−6 wt.% Cu, respectively [7].

The clay mold has lower thermal conductivity (12.75 W/m.K) than the thermal conductivity of carbon steel and stainless steel (56.7 and 16.6 W/m.K, respectively [21]). This discrepancy allows carbon and stainless steel mold to hold the melt temperature by transferring the heat from a disconnected furnace. There was a significant temperature difference between the closest and the farthest observation points in which contributing to the high exponent values of λ_1 and λ_2. In contrast, the clay resists the heat from the mold wall; therefore, a small exponent value is obtained. This work has demonstrated that the λ_1 and λ_2 exponent values of cooling rate, growth rate, and temperature gradient except for local solidification time of directionally solidified Al−4.5 wt.% Cu in the clay mold is smaller than the ones in carbon and stainless steel mold.
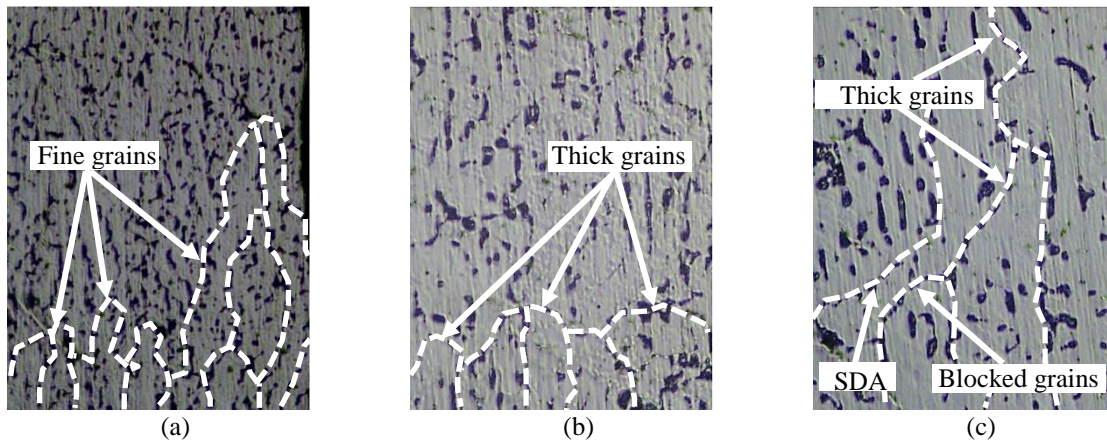
Figure 3. Grain formation across the sample length at: (a) 2.4°C/s, (b) 1.12°C/s, and (c) 0.06°C/s of cooling rates

Table 1. Comparison the exponential of λ_1 as a function of cooling rate

Cu (wt.%)	Linear approach	Growth direction	Mold material	Treatment on the cooling	Ref.
3	$\lambda_1 = 90\,(T_R)^{-0.55}$	downward vertical	stainless steel	Without heating	[5]
4.5	$\lambda_1 = 37.497(T_R)^{-0.238}$	upward vertical	clay	With heating	This work
6	$\lambda_1 = 216\,(T_R)^{-0.55}$	horizontal	stainless steel	Without heating	[8]

Table 2. Comparison exponential of λ_2 as a function of cooling rate, growth rate, and temperature gradient

Cu (wt.%)	Linear approach	Growth direction	Mold material	Treatment on the cooling	Ref.
3	$\lambda_1 = 90\,(T_R)^{-0.55}$ $\lambda_2 = 35\,(V_L)^{2/3}$ $\lambda_2 = 5\,(t_{SL})^{1/3}$				
3	$\lambda_2 = 37\,(T_R)^{-1/3}$	horizontal	carbon steel	without heating	[6]
3	downward vertical	stainless steel	without heating	[5]	[7]
4.5	$\lambda_2 = 16.92(T_R)^{-0.195}$ $\lambda_2 = 15.96(V_L)^{-0.324}$ $\lambda_2 = 6.27(t_{SL})^{0.228}$ $\lambda_2 = 15.96(G)^{-0.324}$	upward vertical	clay	with heating	This work
5	$\lambda_2 = 31\,(V_L)^{-2/3}$	downward vertical	stainless steel	without heating	[5]

	$\lambda_2 = 11 \, (t_{SL})^{1/3}$				
6	$\lambda_1 = 216 \, (T_R)^{-0.55}$ $\lambda_2 = 54.2 \, (T_R)^{-1/3}$	horizontal	stainless steel	without heating	[8]
6	$\lambda_2 = 1.6 \, (G)^{-0.62}$	upward vertical	graphite	quenching	[7]
8	$\lambda_2 = 24 \, (V_L)^{-2/3}$	downward vertical	stainless steel	without heating	[5]
8	$\lambda_2 = 24 \, (V_L)^{-2/3}$	upward vertical	stainless steel	without heating	[9]
10	$\lambda_2 = 22 \, (V_L)^{-2/3}$	upward vertical	stainless steel	without heating	[9]

Micro-hardness

The measured micro-hardness values (HV) as a function of the distance from the heat extraction point is presented in Figure 4. The highest micro-hardness value is 66.49 kg/mm^2 at 5 mm; then, the value decreases slightly to 66.48 kg/mm^2 at 10 mm before gradually decreases and reaches the lowest value 53.42 kg/mm^2 at 50 mm. The micro-hardness values are decreasing with distance. Power law and HP experimental equation 1 (Eq. 1) is applied to address the dependency of HV to the distance from the heat extraction point, and the expression $HV = 71.603x^{-0.054}$ is obtained. The HV exponent value of the distance from the heat extraction point, -0.054 is 0.016 higher than the one obtained by [6] for a different mold material (Table 3).

The decreasing micro-hardness values with the distance are associated with the heat transfer. As the distance increases, it reduces the allowable transferred heat [5]; therefore, the observation point shows a non-uniform temperature. The temperature forms an inclining profile with the distance, and each observed point has a typical cooling line. As for solidification parameters, it is indicated by the decreasing of the cooling rate, growth rate, temperature gradient, and the raised of local solidification time (Figure 2). In addition, the increasing fraction of solid during the cooling process reduces the value of solidification parameters. The solid, which has a lower temperature than the liquid, is more resistant than the liquid; therefore, the increasing fraction of solid reduces the heat transfer efficiency. The decreasing of the heat conductivity of aluminum on the falling of temperature is shown in [21]. These conditions are, on the one hand, promotes the increasing of λ_1 and λ_2; on the other hand, practically decreases the HV (Figure 5a). The similar result of the influence of the solidification parameters on improving the HV has reported by [7,22–26].

$$HV = 71.603x^{-0.054} \quad - \quad R^2 = 0.7131$$
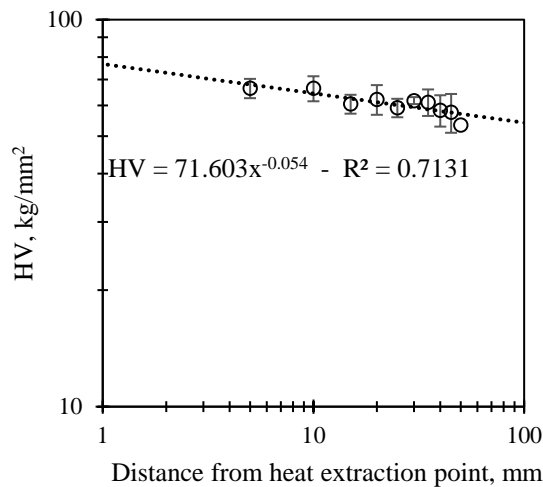
Figure 4. Micro-hardness of Al−4.5wt.%Cu across the length

Table 3. HP experimental equation

Cu (wt.%)	HP expression	HP simplified form	Growth direction	Mold material	Ref.
3	$HV = 41 + 82(\lambda_2)^{-1/2}$	$HV = 94(\lambda_2)^{-0.15}$	vertical downward	stainless steel	[6]
3		$HV = 28.4(\lambda_2)^{-0.21}$	vertical upward	graphite	[7]
4.5	$HV = 94.8(\lambda_2)^{-0.5} + 38.6$	$HV = 103.69(\lambda_2)^{-0.183}$	vertical upward	clay	This work
6		$HV = 44.7(\lambda_2)^{-0.20}$	vertical upward	graphite	[7]
15		$HV = 67.9(\lambda_2)^{-0.17}$	vertical upward	graphite	[7]
24		$HV = 91.6(\lambda_2)^{-0.18}$	vertical upward	graphite	[7]

HV, as the function of the λ_1 and λ_2 is depicted in Figure 5a, b. The λ_1 and λ_2 increases from 23.42 to 77.933 µm and 11.08 to 32.923 µm accordingly. The increase of λ_1 and λ_2 lead to a decreasing in HV. The experimental relation of Hall-Petch and power mathematical expression of Al−4.58wt.%Cu are as follows:

$$HV = 103.69(\lambda_2)^{-0.183}$$

$$HV = 94.8(\lambda_2)^{-0.5} + 38.6$$

High HV is at the minimum λ_1 and λ_2, and it gradually decreases as λ_1 and λ_2 increases. The high cooling rate at the contacted area induces constitutional supercooling, which leads to less grain growth and enhanced grain nucleation. This condition is translated to minimum inter-dendritic spaces. The segregation occurs, and the solute riched layer is created in the liquid front. This layer provides an inter-dendritic liquid denser than the liquid bulk volume of molten metal [27,28]. As the grain grows, the cooling rate, growth rate, and temperature gradient are decreased, providing longer solidification time. The grain growth is enhancing which the increasing of λ_1 and λ_2 indicates [10]. Further, the solute riched liquid in the inter-dendritic region flows toward the dendrite stalks because of gravity [6,29]. The solid becomes much denser near the bottom where λ_1 and λ_2 are at a minimum point, and the density decreases gradually with the distance. The decreasing profile of density is identical to the HV.

The HV exponent value of λ_2 is close to the values in Table 3 for 3, 6, 15, and 24 wt.% compositions of Cu. Some differences in the exponent values are possible because the alloy composition and mold material play an essential role in the solidification mechanism.
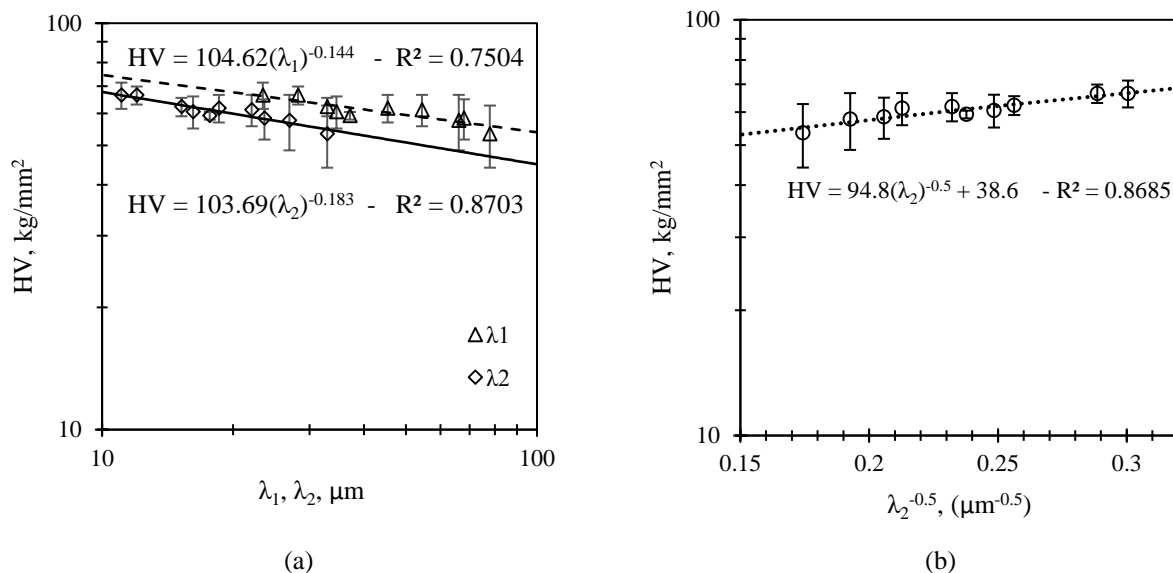
Figure 5. The relation of HV to (a) λ_1 and λ_2, (b) The inverse of the square root of the λ_2 of Al−4.5wt.%Cu

CONCLUSIONS

The microstructure parameters (λ_1 and λ_2) change inversely with the solidification parameters except for t_{SL} and the exponent values of λ_1 and λ_2 are lower than the one with carbon and stainless steel. The micro-hardness value of Al–4.5wt.%Cu decreases with the distance, in contrast with primary dendrite arm spacing (λ_1) and secondary dendrite arm spacing (λ_2). The HV exponent value of λ_2 in the clay mold, -0.183, is close to the one in the graphite mold. These results demonstrate that low thermal conductivity reduces the solidification parameters exponent value of λ_1 and λ_2. Hall-Petch approach was proven the HV exponent value of λ_1 and λ_2 are close for the same type of material. The identical characteristic of clay and graphite provides an option for a potential mold material for further study. Moreover, this study also proposed an HP equation for Al-4.5wt.%Cu, $HV = 38.55 + 94.837(\lambda_2)^{-0.5}$.

ACKNOWLEDGMENTS

REFERENCES

[1]   S. R. Pedapati, D. Paramaguru, M. Awang, H. Mohebbi, and S. Korada, "Effect of process parameters on mechanical properties of AA5052 joints using underwater friction stir welding," *J. Mech. Eng. Sci.*, vol. 14, no. 1, pp. 6259 - 6271, 2020.

[2]   R. Kaufman, "Aluminum Alloy Castings: Properties, Processes, and Applications," in *Elsevier Science*, 2004.

[3]   A. J. Sulaiman H., W. N. W. M. N. Hissyam, A. M. H., M. Ishak, and T. Ariga, "Effect of copper based filler composition on the strength of brazed joint," *J. Mech. Eng. Sci*, vol. 13, no. 2, pp. 5090 - 5103, 2019.

[4]   ASM International Handbook Committee, "Properties and selection--nonferrous alloys and special-purpose materials," in *ASM International Vol 2*. 2001.

[5]   J. E. Spinelli, D. M. Rosa, I. L. Ferreira, A. Garcia, "Influence of melt convection on dendritic spacings of downward unsteady-state directionally solidified Al–Cu alloys," *Mater. Sci. Eng. A*, vol. 383, no. 2, pp. 271 - 282, 2004.

[6]   E. C. Araújo *et al.*, "The Role of Si and Cu Alloying Elements on the Dendritic Growth and Microhardness in Horizontally Solidified Binary and Multicomponent Aluminum-Based Alloys," *Metall. Mater. Trans. A*, vol. 48A, pp. 1163 - 1175, 2017.

[7]   E. Çadirli E. "Effect of solidification parameters on mechanical properties of directionally solidified Al-Rich Al-Cu alloys, " *Met. Mater. Int.*, vol. 19, no. 3, pp. 411 - 422, 2013.

[8]   T. A. Costa *et al*. "Growth direction and Si alloying affecting directionally solidified structures of Al–Cu–Si alloys," *Mater. Sci. Technol.,* vol. 31, no. 9, pp. 1103 - 1112, 2014.

[9]   O. L. Rocha, C. A. Siqueira, A. Garcia, "Heat flow parameters affecting dendrite spacings during unsteady-state solidification of Sn-Pb and Al-Cu alloys, " *Metall. Mater. Trans. A*, vo. 34, no. 4, pp. 995 - 1006, 2003.

[10]   S. Slamet, S., and I. Kusumaningtyas, "Effect of composition and pouring temperature of Cu(20-24)wt.%Sn by sand casting on fluidity and mechanical properties", *J. Mech. Eng. Sci*, vol. 13, no. 4, pp. 6022-6035, 2019.

[11]   D. Masnur, Suyitno and V. Malau, "The Influence of Mold Material on Cooling Curve, Solidification Parameters, and Micro-hardness of Al–6wt .% Si in Unidirectional Solidification," *IOP Conf. Ser. Mater. Sci. Eng.,* pp. 547, 2019.

[12]   S. Shariza, T. J. S. Anand, A. R. M. Warikh, L. C. Chia, C. K. Yau, L. B. Huat, "Bond strength evaluation of heat treated Cu-Al wire bonding," *J. Mech. Eng. Sci.* vol. 12, no. 4, pp. 4275 - 4284, 2018.

[13]   ASM International. "Alloy Phase Diagrams," in *ASM Handbook, Volume 3*, 2004.

[14]   D. Eskin, Q. Du, D. Ruvalcaba and L. Katgerman, "Experimental study of structure formation in binary Al-Cu alloys at different cooling rate," *Mater. Sci. Eng. A*, vo. 405, pp. 1 - 10, 2005.

[15]   W. Desrosin, L. Boycho, V. Scheiber, C. M. Méndez, C. E. Schvezov, A. E. Ares. "Evolution of Metallographic Parameters during Horizontal Unidirectional Solidification of Zn-Sn Alloys," *Procedia Mater. Sci.,* vol. 8, pp. 968 - 977, 2015.

[16]   D. H. Askeland, P. P. Fulay, "Materials Science and Engineering 2nd Editions," in *Cengage Learning,* 2009.

[17]   H. Kaya, U. Böyük, E. Çadirli and N. Maraşli, "Influence of growth rate on microstructure, microhardness, and electrical resistivity of directionally solidified Al-7 wt% Ni hypo-eutectic alloy," *Met. Mater. Int.* vol. 19, no. 1, pp. 39 - 44, 2013.

[18]   T. Chen, X. Li, H. Guo and Y. Hao, "Microstructure and crystal growth direction of Al−Cu alloy," *Trans Nonferrous Met. Soc. China.* vol. 25, no. 5, pp. 1399 - 1409, 2015.

[19]   ASTM Int., "ASTM E384: Standard Test Method for Knoop and Vickers Hardness of Materials," in *ASTM Stand.* 2012.

[20]   W. D. Griffiths, "Heat-transfer coefficient during the unidirectional solidification of an Al-Si alloy casting," *Met. Mater. Trans B*. vol. 30, no. 3, pp. 473 - 482, 1999.

[21]   T. L. Bergman, A. S. Lavine, F. P. Incropere and D. P. DeWitt, "Fundamentals of Heat and Mass Transfer," in *John Wiley & Sons, Inc.*, 2011.

[22]   S. Engin, U. Büyük and N. Maraşli, "The effects of microstructure and growth rate on microhardness, tensile strength, and electrical resistivity for directionally solidified Al-Ni-Fe alloys," *J. Alloys Compd..* vol. 660, pp. 23 - 31, 2016.

[23]   A. Aker and H. Kaya, "Measurements of microstructural, mechanical, electrical, and thermal properties of an Al-Ni Alloy," *Int. J. Thermophys*. vol. 34, no. 2, pp. 267 - 283, 2013.

[24]   H. Kaya, U. Böyük, E. Çadirli E and N. Maraşli, "Measurements of the microhardness, electrical and thermal properties of the Al-Ni eutectic alloy," *Mater. Des.,* vol. 34, pp: 707 - 712, 2012.

[25]   H. Kaya, U. Büyük, E. Çadırlı and N. M. Yildiz, "Influence of growth rate on microstructure, microhardness, and electrical resistivity of directionally solidified Al-7 wt% Ni Hypo-Eutectic Alloy," *Met. Mater. Int.*, vol. 19, pp: 39 - 44, 2013.

[26]   A. Hiremath, A. AmarMurthy, S. V. Pranavathmaja, A. Jajodia and R. Sreenath, "Effect of end chills, reinforcement content and carburization on the hardness of LM25-borosilicate glass particulate composite," *J. Mech. Eng. Sci.* vol. 12, no. 4, pp. 4203 - 4215, 2018.

[27]   K. S. Cruz, I. L. Ferreira, J. E. Spinelli, N. Cheung and A. Garcia, "Inverse segregation during transient directional solidification of an Al – Sn alloy : Numerical and experimental analysis," *Mat. Chem. Phy.* vol. 115, pp. 116 - 121, 2009.

[28]   M. C. Flemmings, "Solidification Processing" in *New York: McGraw-Hill*, 1974.

[29]   I. L. Ferreira, C. A. Santos, V. Voller and A. Garcia, "Analytical , Numerical , and Experimental Analysis of Inverse Macrosegregation during Upward Unidirectional Solidification of Al-Cu Alloys," *Met. Mater. Trans B.* vo. 35, pp. 285 - 297, 2004.